BELLE2-CONF-PH-2022-002
March 11, 2022

Measurements of the branching fraction and direct *CP*-violating asymmetry in $B^0 \to K^0\pi^0$ decays

(Belle II Collaboration)

Abstract

We report measurements of the branching fraction ($\mathcal{B}$) and direct *CP*-violating asymmetry ($\mathcal{A}_{CP}$) in the charmless decays $B^0 \to K^0\pi^0$ at Belle II. A sample of e^+e^- collisions, corresponding to $189.8\,\text{fb}^{-1}$ of integrated luminosity, recorded at the $\Upsilon(4S)$ resonance is used for this study. We find 135^{+16}_{-15} signal candidates, and measure $\mathcal{B}(B^0 \to K^0\pi^0) = [11.0 \pm 1.2(\text{stat}) \pm 1.0(\text{syst})] \times 10^{-6}$ and $\mathcal{A}_{CP} = -0.41^{+0.30}_{-0.32}(\text{stat}) \pm 0.09(\text{syst})$.

1. INTRODUCTION

Decays mediated by flavor-changing neutral currents such as $B^0 \to K^0\pi^0$ are suppressed in the standard model (SM) and provide an indirect route to search for beyond-the-SM physics [1]. The latter is accomplished by checking consistency between measurements and corresponding theory predictions, since new particles may enter the loop affecting various observables. One such observable probed at flavor factories is the asymmetry due to CP violation, which arises because of an irreducible phase in the Cabibbo-Kobayashi-Maskawa (CKM) matrix [2] of the quark sector within the SM.

At Belle II, pairs of neutral B mesons are coherently produced in the process $e^+e^- \to \Upsilon(4S) \to B^0\overline{B}^0$. When one of these mesons decays to a CP eigenstate f_{CP} (e.g. $K^0_S\pi^0$) and the other to a flavor-specific final state $f_{\rm tag}$, the time-dependent decay rate is given as

$$\mathcal{P}(\Delta t) = \frac{\mathrm{e}^{-|\Delta t|/\tau_{B^0}}}{4\tau_{B^0}}[1 + q\{\mathcal{A}_{CP}\cos(\Delta m_d \Delta t) + \mathcal{S}_{CP}\sin(\Delta m_d \Delta t)\}], \quad (1)$$

where $\Delta t = t_{CP} - t_{\rm tag}$ is the proper time difference between the decay into f_{CP} and $f_{\rm tag}$, q is the flavor of $f_{\rm tag}$ being $+1$ (-1) for the B^0 ($\overline{B}^0$) decay to $f_{\rm tag}$, Δm_d is the B^0–$\overline{B}^0$ mixing frequency, and τ_{B^0} is the B^0 lifetime. The quantity $\mathcal{A}_{CP}$ is a measure of direct CP violation, and $\mathcal{S}_{CP}$ denotes CP violation due to interference between decays with and without B^0–$\overline{B}^0$ mixing.

The CKM and color suppression of the tree-level $b \to su\overline{u}$ transition means that $B^0 \to K^0_S\pi^0$ decays are dominated by the top-quark mediated $b \to sd\overline{d}$ loop diagram, which carries a weak phase $\arg(V_{tb}V^*_{ts})$; V_{ij} denote the CKM matrix elements. If subleading contributions are small, $\mathcal{S}_{CP}$ is expected to be equal to $\sin 2\phi_1$ and $\mathcal{A}_{CP} \approx 0$. Further, $B^0 \to K^0_S\pi^0$ decays comprise a key component in improving the sensitivity of an isospin sum-rule proposed by Gronau [3]. The sum rule, given by

$$I_{K\pi} = \mathcal{A}_{K^+\pi^-} + \mathcal{A}_{K^0\pi^+}\frac{\mathcal{B}(K^0\pi^+)}{\mathcal{B}(K^+\pi^-)}\frac{\tau_{B^0}}{\tau_{B^+}} - 2\mathcal{A}_{K^+\pi^0}\frac{\mathcal{B}(K^+\pi^0)}{\mathcal{B}(K^+\pi^-)}\frac{\tau_{B^0}}{\tau_{B^+}} - 2\mathcal{A}_{K^0\pi^0}\frac{\mathcal{B}(K^0\pi^0)}{\mathcal{B}(K^+\pi^-)} = 0, \quad (2)$$

properly accounts for subleading amplitudes by combining the branching fraction ($\mathcal{B}$) and $\mathcal{A}_{CP}$ values measured in B decays to four possible $K\pi$ final states: $K^+\pi^-$, $K^0\pi^+$, $K^+\pi^0$, and $K^0\pi^0$. A precise measurement of $\mathcal{B}$ and $\mathcal{A}_{CP}$ in these channels thus represents an important consistency test of the SM, as described in Eq. (2). Related measurements in $B^0 \to K^0\pi^0$ decays have been reported by Belle [4, 5] and BaBar [6, 7]. With the data size anticipated at Belle II, we expect to have significantly smaller uncertainties compared to what the earlier two experiments have achieved for these quantities.

In this document, we report measurements of $\mathcal{B}$ and $\mathcal{A}_{CP}$ in $B^0 \to K^0\pi^0$ decays conducted using a time-dependent analysis at Belle II. As our focus is more on $\mathcal{A}_{CP}$ than $\mathcal{S}_{CP}$ coupled with limited data sample available, we fix the $\mathcal{S}_{CP}$ value to its world average in $B^0 \to K^0_S\pi^0$ decays [8].

2. THE BELLE II DETECTOR AND DATA SAMPLE

Belle II [9] is a particle spectrometer with almost 4π solid-angle coverage, designed to reconstruct final-state particles of e^+e^- collisions delivered by the SuperKEKB asymmetric-energy collider [10], located at the KEK laboratory in Tsukuba, Japan. The energies of

the positron and electron beams are 4 and 7 GeV, respectively. Belle II comprises a number of subdetectors surrounding the interaction point (IP) in a cylindrical geometry. The innermost one is the vertex detector (VXD), which uses position-sensitive silicon layers to sample the trajectories of charged particles ('tracks') in the vicinity of the interaction region to extrapolate the decay positions of their long-lived parent particles. The VXD includes two inner layers of DEPFET-based pixel sensors and four outer layers of double-sided microstrip sensors. The second pixel layer is currently incomplete covering one sixth of the azimuthal angle. Charged-particle momenta and charges are measured by a large-radius, helium-ethane, small-cell central drift chamber (CDC), which also offers charged-particle-identification information via a measurement of specific ionization. A Cherenkov-light angle and time-of-propagation (TOP) detector surrounding the CDC provides charged-particle identification in the central detector volume, supplemented by proximity-focusing, aerogel, ring-imaging Cherenkov (ARICH) detectors in the forward region with respect to the electron beam. A CsI(Tl)-crystal electromagnetic calorimeter (ECL) provides electron-energy measurements and photon reconstruction. A solenoid surrounding the ECL generates a uniform axial 1.5 T magnetic field filling its inner volume. Layers of plastic scintillators and resistive-plate chambers, interspersed between the magnetic flux-return iron plates, allow for the identification of K_L^0 and muons. The subdetectors most relevant for our study are the VXD, CDC, and ECL.

The data sample used in the study consists of all good-quality runs collected at a center-of-mass (CM) energy near the $\Upsilon(4S)$ resonance, corresponding to an integrated luminosity of $189.8\,\mathrm{fb}^{-1}$. We use large samples of simulated $e^+e^- \to q\bar{q}$ ($q = u, d, s, c$), $\Upsilon(4S) \to B^0\overline{B}^0$ and B^+B^- events to optimize the event selection and study possible background contributions. We also use Monte Carlo (MC) signal events to determine signal models and estimate the selection efficiency.

The B-meson decays are simulated with the EvtGen generator [11], and the effect of final-state radiation is simulated by the Photos package [12]. The simulation of $e^+e^- \to q\bar{q}$ continuum background uses the KKMC generator [13] interfaced to Pythia [14]. The interactions of final-state particles with the detector are simulated using Geant4 [15].

3. RECONSTRUCTION AND SELECTION

Charged-particle tracks are reconstructed with the VXD and CDC. Photons are identified as isolated ECL clusters that are not matched to any track. The K_S^0 candidates are reconstructed from pairs of oppositely charged tracks having an invariant mass between 482 and $513\,\mathrm{MeV}/c^2$. We reconstruct π^0 candidates from pairs of photons that have energies greater than 80 and 223 MeV if detected in the ECL barrel and endcap, respectively. The selection also requires the π^0 mass to lie between 119 and $150\,\mathrm{MeV}/c^2$ and the absolute cosine of its π^0 helicity angle to be less than 0.953. These criteria suppress contributions from misreconstructed π^0 candidates.

The B-meson candidate is reconstructed by combining a K_S^0 with a π^0 candidate. For this purpose, we use two kinematic variables: the beam-energy-constrained mass (M_{bc}) and the energy difference (ΔE), defined as

$$M_{\mathrm{bc}} = \sqrt{E_{\mathrm{beam}}^2 - \vec{p}_B^{\,2}}, \qquad (3)$$
$$\Delta E = E_B - E_{\mathrm{beam}},$$

where $E_{\rm beam}$ is the beam energy, E_B and $\vec{p}_B$ are respectively the reconstructed energy and momentum of the B meson; all calculated in the CM frame. We retain candidate events satisfying $5.24 < M_{\rm bc} < 5.29$ GeV/c^2 and $|\Delta E| < 0.3$ GeV.

The presence of a high momentum π^0 causes a nontrivial correlation between $M_{\rm bc}$ and ΔE owing to the shower leakage of final-state photons. To reduce the correlation with ΔE we use the following modified version of $M_{\rm bc}$, calculated from the beam energy and momenta of final-state particles as:

$$M'_{\rm bc} = \sqrt{E^2_{\rm beam} - \left(\vec{p}_{K^0_S} + \frac{\vec{p}_{\pi^0}}{|\vec{p}_{\pi^0}|}\sqrt{(E_{\rm beam} - E_{K^0_S})^2 - m^2_{\pi^0}}\right)^2}, \tag{4}$$

where all kinematic quantities are again calculated in the CM frame. We will refer to $M'_{\rm bc}$ as just $M_{\rm bc}$ henceforth in this document.

As shown in Eq. (1), one of the important parameters to calculate the time-dependent decay rate is Δt. We find that its error ($\Delta t_{\rm err}$) has a significant tail as shown in Fig. 1, caused by K^0_S decays outside the VXD that lead to a poor decay time resolution. To suppress such events we restrict $\Delta t_{\rm err}$ to be less than 2.5 ps.

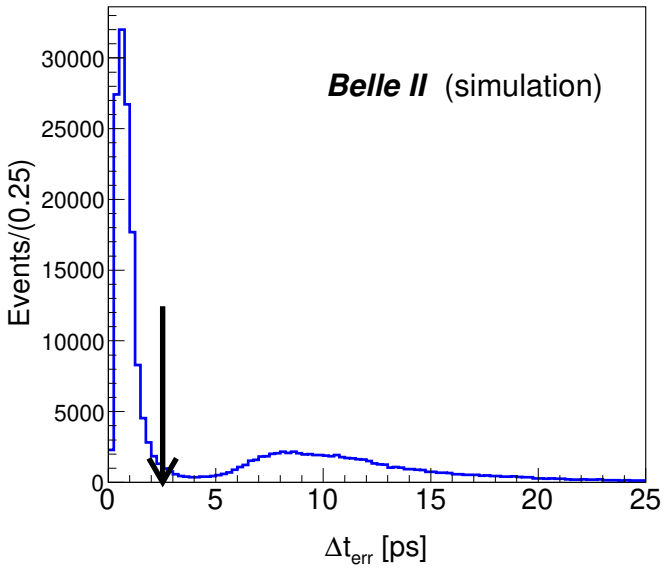

FIG. 1. Distribution of $\Delta t_{\rm err}$ obtained for signal events after applying all the criteria described above. The downward arrow indicates the position of the $\Delta t_{\rm err}$ selection.

The most dominant source of background is from $e^+e^- \to q\bar{q}$ continuum process. These events result in final-state particles collimated into two back-to-back jets, whereas those from $e^+e^- \to \Upsilon(4S) \to B\overline{B}$ are uniformly distributed over the 4π solid angle. We exploit this difference in event topology to suppress continuum background. We combine a set of 39 variables, known to provide discrimination between B-meson signal and continuum background, using a boosted-decision-tree (BDT) classifier [16]. For this purpose, we use $e^+e^- \to q\bar{q}$, $B^0\overline{B}^0$ and B^+B^- MC events, each equivalent to an integrated luminosity of $1\,{\rm ab}^{-1}$. The BDT output ($C_{\rm out}$) distribution shown in Fig. 2 clearly discriminates the signal from background events. As it is difficult to analytically model the $C_{\rm out}$ shape, we translate

it into a new variable:

$$C'_{\rm out} = \ln\left(\frac{C_{\rm out} - C_{\rm out,min}}{C_{\rm out,max} - C_{\rm out}}\right), \tag{5}$$

which can be parametrized by one or more Gaussian functions. Here, $C_{\rm out,min} = 0.6$ and $C_{\rm out,max} \simeq 1$. With the $C_{\rm out,min}$ criterion, we reject about 89% of the continuum background with a 18% relative loss in signal efficiency.

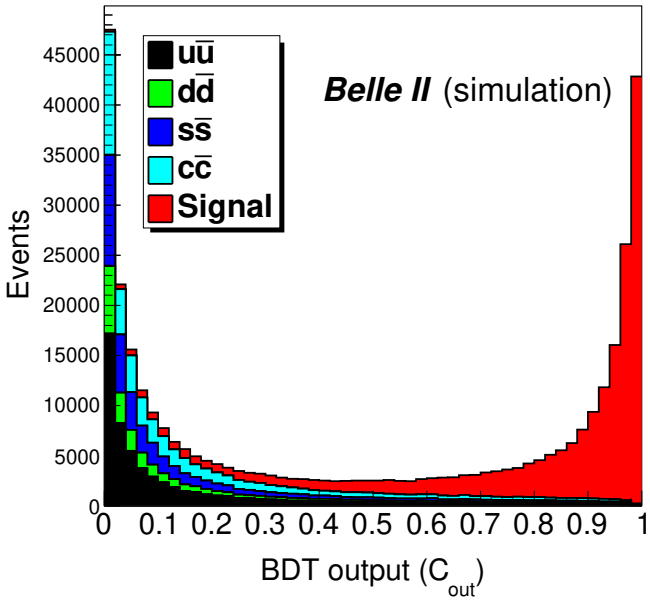

FIG. 2. Distributions of BDT output obtained for signal and background MC events.

After the final selection and background suppression, we find that the average number of B candidates per event is 1.009. The multiple candidates mostly arise due to a random combination of final-state particles. To select the best candidate in events with multiple candidates, we first compare the π^0 mass-constrained fit χ^2 probability ('p-value'). In case there are more than one candidates sharing the same π^0 mass-constrained fit p-value, we pick up the one with the best K^0_S vertex fit p-value. Our best candidate selection retains 74% of the time the correct B candidate in events with multiple B candidates.

The efficiency of correctly reconstructed signal events after all the selection is 12.3%, and the fraction of self cross-feed (SCF) events is 1.5%. As the SCF fraction is small, we consider both correctly reconstructed and SCF events as part of the signal.

To facilitate a time-dependent analysis in absence of any charged particles directly coming from the B^0 meson, we make use of the interaction point (IP) constraint for inferring the B^0 decay vertex. For this, the flight direction of each K^0_S candidate is required to be consistent with the direction of its vertex displacement with respect to the IP. On the other hand, the tag-side vertex is obtained using well-reconstructed tracks that are not assigned to the $B^0 \to K^0_S\pi^0$ decay. We determine the flavor of the tag-side B meson (q) from properties of particles that are not associated with the reconstructed $B^0 \to K^0_S\pi^0$ decay. The Belle II flavor tagging algorithm [17] returns, as the tagging decision, $q = +1$ (-1) when the tagged B meson is a B^0 ($\overline{B}^0$), and the tagging dilution, r that ranges from 0 (no flavor discrimination) to 1 (unambiguous flavor assignment).

4. SIGNAL EXTRACTION

We obtain the signal yield and *CP* asymmetry from a four-dimensional (4D) unbinned extended maximum-likelihood fit to $M_{\rm bc}$, ΔE, $C'_{\rm out}$, and Δt. For the signal component, $M_{\rm bc}$ is modeled with the sum of a Crystal Ball (CB) [18] and a Gaussian function with common mean, ΔE with the sum of a CB and a double Gaussian function with common mean, and $C'_{\rm out}$ with the sum of an asymmetric and a regular Gaussian function. The Δt probability density function (PDF) is given by

$$\mathcal{P}_{\rm sig}(\Delta t, q) = \frac{e^{-|\Delta t|/\tau_{B^0}}}{4\tau_{B^0}}[\{1 - q\Delta w_r + q\mu_r(1-2w_r)\} + \{q(1-2w_r) + \mu_r(1 - q\Delta w_r)\} \\ \{\mathcal{A}_{CP}\cos(\Delta m_d \Delta t) + \mathcal{S}_{CP}\sin(\Delta m_d \Delta t)\}] \otimes \mathcal{R}_{\rm sig}, \quad (6)$$

where w_r is the wrong tag fraction, Δw_r is the difference in w_r between B^0 and $\overline{B}^0$, μ_r is the difference in their tagging efficiency, and $\mathcal{R}_{\rm sig}$ is the proper time resolution function, composed of a double Gaussian. We set τ_{B^0} to 1.520 ps and Δm_d to 0.507 ps^{-1} [8]. The data are divided into seven $q \cdot r$ bins with the tagging parameters for each bin (w_r, Δw_r, and μ_r) fixed to the respective values obtained in Ref. [17]. All signal PDF shapes are fixed to the values determined from a $q \cdot r$ binned fit to signal MC events. For the continuum background component, an ARGUS function [19] is used for $M_{\rm bc}$, a linear function for ΔE, and the sum of an asymmetric and a regular Gaussian function for $C'_{\rm out}$. Its Δt distribution is modeled with an exponential function convolved with a Gaussian for the tail; we use a double Gaussian for its resolution function ($\mathcal{R}_{q\overline{q}}$). For the continuum background component, we float the PDF shape parameters common over the $q \cdot r$ bins. For the $B\overline{B}$ background component, a two-dimensional Kernel estimation PDF [20] is used to model both ΔE and $M_{\rm bc}$ distributions, and the sum of an asymmetric and a regular Gaussian function is used for $C'_{\rm out}$. Its Δt distribution is modeled with an exponential function convolved with a Gaussian for the tail; we again use a double Gaussian for its resolution function ($\mathcal{R}_{B\overline{B}}$). The $B\overline{B}$ background shape are fixed from the overall MC fit.

The free parameters in our final fit are the signal yield, $\mathcal{A}_{CP}$, Gaussian-constrained $B\overline{B}$ background yield, continuum background yield, $M_{\rm bc}$ ARGUS parameter, ΔE slope, and $C'_{\rm out}$ relative width for the $q\overline{q}$ component. The $\mathcal{S}_{CP}$ value fixed to its world average [8]. We correct the $M_{\rm bc}$, ΔE, and $C'_{\rm out}$ PDF shapes for possible data-MC differences, according to the values obtained with a control sample of $B^+ \to \overline{D}^0(\to K^+\pi^-\pi^0)\pi^+$.

We use a control sample $B^0 \to J/\psi\, K^0_S$ to validate the time-dependent analysis framework. To mimic the signal decay, we do not vertex the two charged leptons coming from the J/ψ decay. The obtained values of the B^0 lifetime, $\mathcal{A}_{CP}$, and $\mathcal{S}_{CP}$ are found to be consistent with their world average [8]. The same sample is also used to correct the Δt PDF shape parameters for possible data-MC differences.

Figure 3 shows the sum of projections for the seven $q \cdot r$-binned 4D fit, where the signal region criteria ($5.27 < M_{\rm bc} < 5.29\,{\rm GeV}/c^2$, $-0.15 < \Delta E < 0.10\,{\rm GeV}$, and $C'_{\rm out} > 0.0$) are applied on all but for the variable plotted. The obtained signal yield is 135^{+16}_{-15}, where the quoted uncertainty is statistical only. We also find 2214^{+49}_{-48} and 44 ± 5 events for the $q\overline{q}$ and $B\overline{B}$ background, respectively. The $B^0 \to K^0\pi^0$ branching fraction and direct *CP* asymmetry are measured to be $(11.0 \pm 1.2 \pm 1.0) \times 10^{-6}$ and $0.41^{+0.30}_{-0.32} \pm 0.09$, respectively. The first uncertainties are statistical and the second are systematic (described below). This is an improved measurement of $\mathcal{B}$ and $\mathcal{A}_{CP}$ in $B^0 \to K^0\pi^0$ decays compared to the previous Belle II result [21] where a time-integrated study was performed to determine the $\mathcal{A}_{CP}$ value.

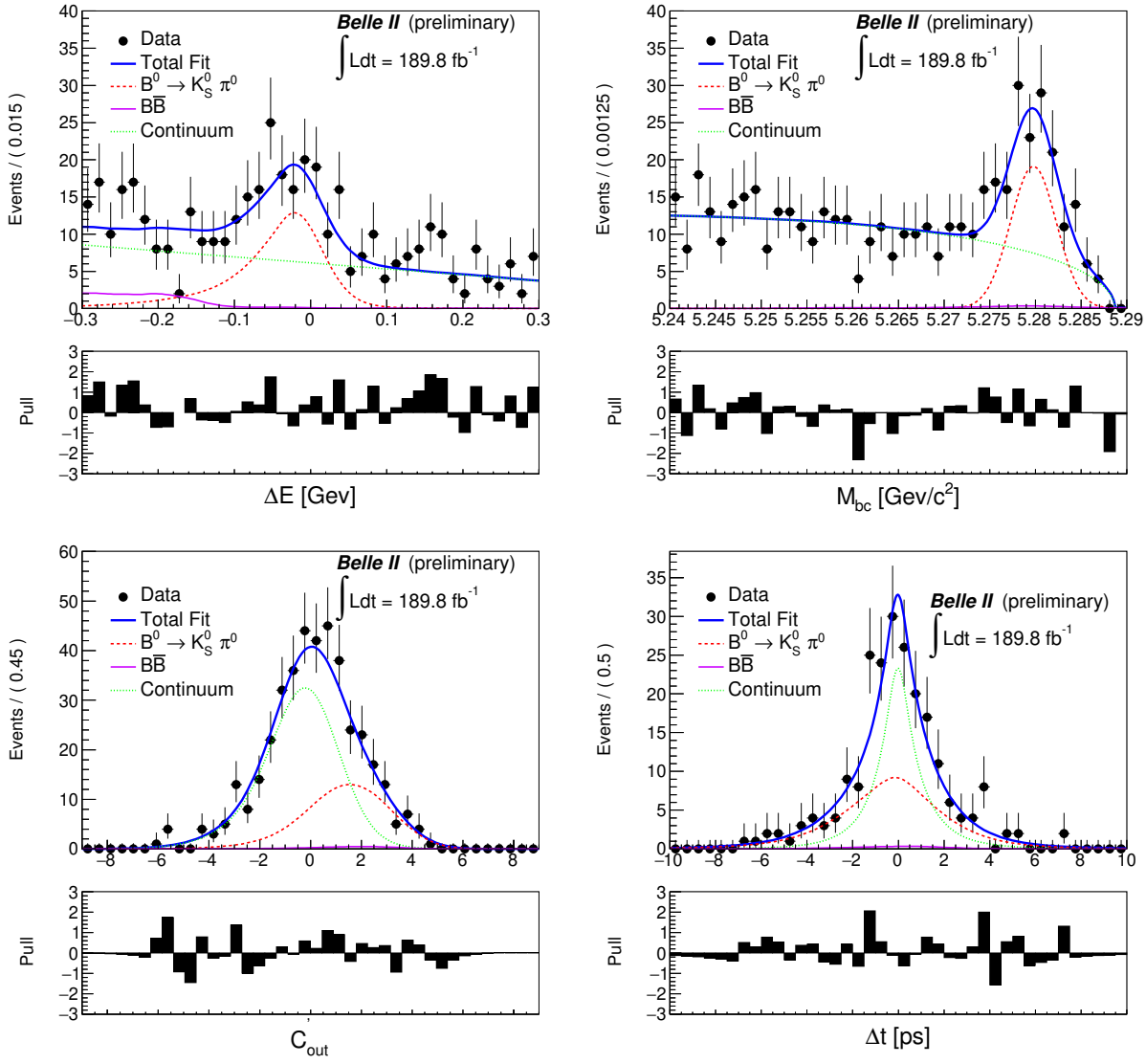

FIG. 3. Signal enhanced 4D fit projections for the $q \cdot r$ integrated sample.

5. SYSTEMATIC UNCERTAINTIES

Various sources of systematic uncertainties contributing to the branching fraction and direct *CP* asymmetry are reported in Tables I and II, respectively. We assume these sources to be independent and add their contributions in quadrature to get the total systematic uncertainty.

5.1. Systematic uncertainties on the branching fraction

- **Tracking efficiency:** The systematic uncertainty due to possible data-MC discrepancies in the reconstruction of charged particles is 0.3% for per track[22]. We linearly add this uncertainty corresponding to each of the two pion tracks coming from the K_S^0 decay in the signal side.

- **K_S^0 reconstruction efficiency:** From a data-MC comparison of the K_S^0 yield, we find that the ratio of K_S^0 reconstruction efficiency changes almost linearly as a function of its flight length [22]. We apply an uncertainty of 0.4% for each centimeter of the average flight length of K_S^0 candidates resulting in a 4.2% total systematic uncertainty.

- **π^0 reconstruction efficiency:** We estimate the systematic uncertainty due to possible data-MC discrepancies in the π^0 reconstruction and selection using inclusive decay samples of $D^0 \to K^-\pi^+\pi^0$ and $D^0 \to K^-\pi^+$. The data-MC efficiency ratio is found to be close to unity with an uncertainty of 7.5%, which we assign as the systematic uncertainty.

- **Continuum suppression efficiency:** We evaluate possible data-MC differences in the continuum-suppression efficiency using a control sample of $B^+ \to \overline{D}^0(\to K^+\pi^-\pi^0)\pi^+$. As the ratio of efficiency obtained in data and simulation is close to unity, the statistical uncertainty on the efficiency ratio (1.6%) is assigned as the systematic uncertainty.

- **$B\overline{B}$ pair counting:** An overall uncertainty of 3.2% is taken as a systematic uncertainty on the number of $B\overline{B}$ used, which includes the uncertainty on the $\Upsilon(4S) \to B^0\overline{B}^0$ branching fraction (f^{00}), cross section, integrated luminosity, and potential shifts from the peak CM energy during run periods.

- **Signal and background modeling:** The uncertainties due to signal PDF shape are estimated by varying the correction factors by $\pm 1\sigma$ of their statistical uncertainty. Similarly, the uncertainties due to background PDF shape are calculated by varying all fixed parameters by $\pm 1\sigma$, determined from MC component fit. We fix the $M_{\rm bc}$ ARGUS endpoint to the value obtained from the sideband data. Later we vary it by $\pm 1\sigma$ (according to the error in data) to assign a systematic uncertainty.

- **Fit bias:** Potential fit bias is checked by performing an ensemble test comprising 1000 pseudoexperiments in which signal events are drawn from the corresponding MC sample and background events are generated according to their PDF shapes. We calculate the mean shift of signal yield from the input value and assign it as a systematic uncertainty.

- **Physics parameters:** Physics parameters τ_{B^0}, Δm_d, and $\mathcal{S}_{CP}$ are fixed to their world average values in the fit. The systematic uncertainty is thus estimated by varying their uncertainties by $\pm 1\sigma$.

5.2. Systematic uncertainties on $\mathcal{A}_{CP}$

- **Flavor tagging:** Systematic error due to uncertainties in the wrong tag fraction is estimated by varying the parameters individually for each $q \cdot r$ region by their 1σ uncertainties.

- **Resolution function:** Systematic error due to uncertainties in the resolution function is estimated by varying each resolution parameter obtained from data by their 1σ uncertainties.

TABLE I. List of systematic uncertainties contributing to the measured branching fraction.

Source	$\delta\mathcal{B}$ (%)
Tracking efficiency	0.6
K^0_S reconstruction efficiency	4.2
π^0 reconstruction efficiency	7.5
Continuum suppression efficiency	1.6
Number of $B\overline{B}$ events	3.2
Signal modeling	1.0
Background modeling	0.9
Possible fit bias	2.0
Physics parameters	0.4
Total	9.6

- **Physics parameters:** Physics parameters τ_{B^0}, Δm_d, and $\mathcal{S}_{CP}$ are fixed to their world average in the fit. Therefore, the systematic uncertainty is estimated by varying their uncertainties by $\pm 1\sigma$.

- ***B* decay background asymmetry:** In the nominal fit, we assume the charmless B decay background to be CP symmetric. However, there could be a nontrivial asymmetry arising due to this component. To take such possibility into account, we use an alternative Δt PDF given by

$$\mathcal{P}_{B\overline{B}}(\Delta t, q) = \frac{\mathrm{e}^{-|\Delta t|/\tau_{B^0}}}{4\tau_{B^0}}[1 + q\{\mathcal{A}_{CP}\cos(\Delta m_d \Delta t) + \mathcal{S}_{CP}\sin(\Delta m_d \Delta t)\}] \otimes R_{B\overline{B}}, \quad (7)$$

  instead of the exponential function. We perform two different fits by setting $\mathcal{S}_{CP}$ to either $+1$ or -1, and $\mathcal{A}_{CP} = 0.0$. We then calculate the deviations in $\mathcal{A}_{CP}$ value from the nominal fit. These deviations are assigned as a systematic uncertainty due to B decay background asymmetry. We estimate this systematic in $B^0 \to J/\psi K^0_S$ data themselves.

- **Fit bias:** Potential fit bias is checked by performing an ensemble test comprising 1000 pseudoexperiments in which signal events are drawn from the corresponding MC sample and background events are generated according to their PDF shapes. We calculate the mean shift of $\mathcal{A}_{CP}$ from its input value and assign it as a systematic uncertainty.

- **Tag-side interference:** Systematic uncertainties arising from unaccounted for tag-side interference effects are taken from Ref. [23].

- **Signal and background modeling:** The uncertainties due to signal and background PDF shape are estimated in a manner similar to the branching fraction case.

- **VXD misalignment:** The systematic uncertainty is taken from Ref. [24].

TABLE II. List of systematic uncertainties contributing to $\mathcal{A}_{CP}$.

Source	$\delta\mathcal{A}_{CP}$
Flavor tagging	0.040
Resolution function	0.050
Physics parameter	0.021
B decay background asymmetry	0.002
Possible fit bias	0.010
Tag-side interference	0.038
Background modeling	0.004
Signal modeling	0.015
VXD misalignment	0.033
Total	0.086

6. RESULTS AND SUMMARY

We report measurements of the branching fraction and direct CP asymmetry based on 189.8 fb^{-1} data sample collected near the $\Upsilon(4S)$ resonance by the Belle II detector. The observed signal yield is 135^{+16}_{-15}. We measure $\mathcal{A}_{CP} = -0.41^{+0.30}_{-0.32}(\text{stat})\pm0.09(\text{syst})$ and $\mathcal{B}(B^0 \to K^0\pi^0) = [11.0 \pm 1.2(\text{stat}) \pm 1.0(\text{syst})] \times 10^{-6}$. This is the first measurement of $\mathcal{A}_{CP}$ in $B^0 \to K^0\pi^0$ decays by Belle II performed with a time-dependent analysis. The results agree with previous determinations [21].

7. ACKNOWLEDGEMENT

We thank the SuperKEKB group for the excellent operation of the accelerator; the KEK cryogenics group for the efficient operation of the solenoid; the KEK computer group for on-site computing support; and the raw-data centers at BNL, DESY, GridKa, IN2P3, and INFN for off-site computing support. This work was supported by the following funding sources: Science Committee of the Republic of Armenia Grant No. 20TTCG-1C010; Australian Research Council and research grant Nos. DP180102629, DP170102389, DP170102204, DP150103061, FT130100303, FT130100018, and FT120100745; Austrian Federal Ministry of Education, Science and Research, Austrian Science Fund No. P 31361-N36, and Horizon 2020 ERC Starting Grant no. 947006 "InterLeptons"; Natural Sciences and Engineering Research Council of Canada, Compute Canada and CANARIE; Chinese Academy of Sciences and research grant No. QYZDJ-SSW-SLH011, National Natural Science Foundation of China and research grant Nos. 11521505, 11575017, 11675166, 11761141009, 11705209, and 11975076, LiaoNing RevitaJHEP 10 (2014) 165lization Talents Program under contract No. XLYC1807135, Shanghai Municipal Science and Technology Committee under contract No. 19ZR1403000, Shanghai Pujiang Program under Grant No. 18PJ1401000, and the CAS Center for Excellence in Particle Physics (CCEPP); the Ministry of Education, Youth and Sports of the Czech Republic under Contract No. LTT17020 and Charles University grants SVV 260448 and GAUK 404316; European Research Council, 7th Framework PIEF-GA-2013-622527, Horizon 2020 ERC-Advanced Grants No. 267104 and 884719, Horizon 2020 ERC-Consolidator Grant No. 819127, Horizon 2020 Marie Sklodowska-Curie

grant agreement No. 700525 'NIOBE,' and Horizon 2020 Marie Sklodowska-Curie RISE project JENNIFER2 grant agreement No. 822070 (European grants); L'Institut National de Physique Nucléaire et de Physique des Particules (IN2P3) du CNRS (France); BMBF, DFG, HGF, MPG, and AvH Foundation (Germany); Department of Atomic Energy under Project Identification No. RTI 4002 and Department of Science and Technology (India); Israel Science Foundation grant No. 2476/17, United States-Israel Binational Science Foundation grant No. 2016113, and Israel Ministry of Science grant No. 3-16543; Istituto Nazionale di Fisica Nucleare and the research grants BELLE2; Japan Society for the Promotion of Science, Grant-in-Aid for Scientific Research grant Nos. 16H03968, 16H03993, 16H06492, 16K05323, 17H01133, 17H05405, 18K03621, 18H03710, 18H05226, 19H00682, 26220706, and 26400255, the National Institute of Informatics, and Science Information NETwork 5 (SINET5), and the Ministry of Education, Culture, Sports, Science, and Technology (MEXT) of Japan; National Research Foundation (NRF) of Korea Grant Nos. 2016R1-D1A1B01010135, 2016R1D1A1B02012900, 2018R1A2B3003643, 2018R1A6A1A06024970, 2018R1D1A1B07047294, 2019K1A3A7A09033840, and 2019R1I1A3A01058933, Radiation Science Research Institute, Foreign Large-size Research Facility Application Supporting project, the Global Science Experimental Data Hub Center of the Korea Institute of Science and Technology Information and KREONET/GLORIAD; Universiti Malaya RU grant, Akademi Sains Malaysia and Ministry of Education Malaysia; Frontiers of Science Program contracts FOINS-296, CB-221329, CB-236394, CB-254409, and CB-180023, and SEP-CINVESTAV research grant 237 (Mexico); the Polish Ministry of Science and Higher Education and the National Science Center; the Ministry of Science and Higher Education of the Russian Federation, Agreement 14.W03.31.0026, and the HSE University Basic Research Program, Moscow; University of Tabuk research grants S-0256-1438 and S-0280-1439 (Saudi Arabia); Slovenian Research Agency and research grant Nos. J1-9124 and P1-0135; Agencia Estatal de Investigacion, Spain grant Nos. FPA2014-55613-P and FPA2017-84445-P, and CIDEGENT/2018/020 of Generalitat Valenciana; Ministry of Science and Technology and research grant Nos. MOST106-2112-M-002-005-MY3 and MOST107-2119-M-002-035-MY3, and the Ministry of Education (Taiwan); Thailand Center of Excellence in Physics; TUBITAK ULAKBIM (Turkey); Ministry of Education and Science of Ukraine; the US National Science Foundation and research grant Nos. PHY-1807007 and PHY-1913789, and the US Department of Energy and research grant Nos. DE-AC06-76RLO1830, DE-SC0007983, DE-SC0009824, DE-SC0009973, DE-SC0010073, DE-SC0010118, DE-SC0010504, DE-SC0011784, DE-SC0012704, DE-SC0021274; and the Vietnam Academy of Science and Technology (VAST) under grant DL0000.05/21-23.

[1] E. Kou et al. (Belle II Collaboration), PTEP **2019**, 123C01 (2019), arXiv-1808.10567.

[2] N. Cabibbo, Phys. Rev. Lett. **10**, 531 (1963); M. Kobayashi and T. Maskawa, Prog. Theor. Phys. **49**, 652 (1973).

[3] M. Gronau, Phys. Lett. B **627**, 82 (2005).

[4] Y. Chao et al. (Belle Collaboration), Phys. Rev. D **69**, 111102 (2004).

[5] K. F. Chen et al. (Belle Collaboration), Phys. Rev. D **72**, 012004 (2005).

[6] B. Aubert et al. (BaBar Collaboration), Phys. Rev. Lett. **93**, 131805 (2004).

[7] B. Aubert et al. (BaBar Collaboration), Phys. Rev. D **71**, 111102 (2005).

[8] Y. Amhis et al. (Heavy Flavor Averaging Group), Eur. Phys. J. C (2021) 81:226, arXiv:1909.12524.
[9] T. Abe et al. (Belle II Collaboration), arXiv:1011.0352.
[10] K. Akai, K. Furukawa, and H. Koiso (SuperKEKB Group), Nucl. Instrum. Meth. A **907**, 188 (2018).
[11] D. Lange, Nucl. Instrum. Meth. A **462**, 152 (2001).
[12] E. Barberio et al., Comp. Phys. Comm. **66**, 115 (1991).
[13] B. Ward, S. Jadach and Z. Was, Nucl. Phys. B Proc. Suppl. **116**, 73 (2003)
[14] T. Sjöstrand, S. Mrenna, and P. Skands, Comp. Phys. Comm. **178**, 852 (2008).
[15] S. Agostinelli et al., Nucl. Instrum. Meth. A **506**, 250 (2003).
[16] T. Keck, arXiv:1609.06119.
[17] F. Abudinén et al. (Belle II Collaboration), arXiv:2110.00790
[18] T. Skwarnicki, PhD thesis, INP Krakow, DESY-F31-86-02 (1986).
[19] H. Albrecht et al. (ARGUS Collaboration), Phys. Lett. B **241**, 278 (1990).
[20] K. S. Cranmer, Comp. Phys. Comm. **136**, 198 (2001).
[21] F. Abudinén et al. (Belle II Collaboration), arXiv:2104.14871.
[22] V. Bertacchi et al. (Belle II Tracking Group), arXiv:2003.12466.
[23] I. Adachi et al. (Belle Collaboration), Phys. Rev. Lett. **108**, 171802 (2012)
[24] L. Šantelj et al. (Belle Collaboration), JHEP **10** (2014) 165.